Available online at www.sciencedirect.com
SCIENCE DIRECT®
Journal of Sound and Vibration 290 (2006) 820–838
JOURNAL OF SOUND AND VIBRATION
www.elsevier.com/locate/jsvi

Free vibration of elastically coupled dual-span curved beams

Chris H. Riedel[a,*], Bongsu Kang[b]

[a]*Lawrence Technological University, Mechanical Engineering Department, Southfield, MI 48075, USA*
[b]*Indiana University-Purdue University, Mechanical Engineering Department, Fort Wayne, IN 46805, USA*

Received 12 January 2004; received in revised form 5 April 2005; accepted 26 April 2005
Available online 14 July 2005

Abstract

The free vibration response of dual-span extensional and inextensional circular curved beams constrained by an intermediate elastic support is studied. The elastic constraint consists of a transverse and rotational spring, as well as a tangential spring, which couples the extensional motion of one span with the other. Wave propagation techniques are used to formulate the eigenvalue problem, which result in exact eigensolutions. The effects of the support type and stiffness on the transverse and tangential modes are examined. In addition, the influence of the curvature on the free response of the extensional curved beam is also addressed. For certain support conditions, the extensional and inextensional curved beams have similar behavior. In general, however, the behavior of the system is shown to depend strongly on the type of support, the modeling of the beam as extensional or inextensional, and whether the natural frequencies are above or below the cut-off frequency.

1. Introduction

The vibration of planar curved beams, arches and rings have been the subject of numerous studies due to their wide variety of potential applications, such as bridges, aircraft structures, and turbomachinery blades. These structures are modeled as either extensional (including the extension of the neutral axis) or inextensional (neglecting the extension of the neutral axis). Literature reviews on the vibration of curved beams, rings and arches are found in Refs. [1–3].

*Corresponding author. Tel.: +1 248 204 2570; fax: +1 248 204 2576.
E-mail addresses: riedel@ltu.edu (C.H. Riedel), kang@engr.ipfw.edu (B. Kang).

0022-460X/$ - see front matter © 2005 Elsevier Ltd. All rights reserved.
doi:10.1016/j.jsv.2005.04.016

While most studies of curved beams focus on single spans with classical boundary conditions, in some applications, multiple spans and elastic supports are encountered. As a result, curved beams with elastic supports and multiple spans have also been addressed. Wasserman [4] determined the exact expressions for the lowest natural frequency and critical load of single-span circular arches with flexible boundary conditions. Wang and Lee [5] presented a dynamic slope-deflection method for the free vibration of multi-span circular frames. Filipich et al. [6] studied the vibration of an arch elastically restrained against rotation at one end and with an intermediate support. They solved the problem using three different methods. Petyt and Fleischer [7] studied multi-span curved beam using finite elements and confirmed their results experimentally. Culver and Oestel [8] used the Rayleigh–Ritz method together with the Lagrange multiplier concept to determine the natural frequencies of a two-span horizontally curved beam.

The above studies, however, focus on solution methods rather than physical behavior. For multi-span systems, the coupled response can be quite complex and can depend on many factors. When studying the vibration of curved beams, one of the primary issues to consider is whether the beam is modeled as extensional or inextensional. The extensional model includes the stretching of the neutral axis during vibration, while the inextensional model neglects the stretching of the neutral axis. This fundamental difference results in each model having its own unique characteristics. For example, wave analyses have shown that a cut-off frequency exists for the extensional model, and that the behavior of the extensional model above and below the cut-off frequency is quite different [17]. For the inextensional model, no cut-off frequency exits. It would be expected then that the coupled response of multi-span curved beams would depend strongly on whether the beams are modeled as extensional or inextensional.

Another important issue for multi-span beam systems is the issue of coupling. This interaction between spans can have a significant affect on the overall behavior of the system. For example, it is well known that for weakly coupled, nearly periodic systems, the modes can be highly localized to one span if a small disorder is introduced into the system. This phenomenon is known as mode localization and it has been studied on many physical systems [9–11]. The occurrence and degree of mode localization has been shown to depend on both the disorder and the type of coupling that exists between the spans [12–14]. Thus, both the modeling of the curved beam and its supports may have a significant affect in determining the free vibration response of multi-span curved beam systems.

The purpose of this paper is to study the coupled, free vibration response of a two-span curved beam. The coupling of the spans is through an intermediate elastic support, which consists of a transverse, tangential and rotational spring. The eigenvalue problem is formulated using wave propagation techniques. These techniques include both propagating and attenuating wave components, which results in the formulation being exact. The effects of the elastic support on the coupled response of both extensional and inextensional curved beam models are studied. In general, it is found that each type of elastic support affects the curved beam system differently. It is also observed that the behavior of the extensional and inextensional models is, in general, different. However, under certain conditions, they can exhibit similar behavior. The exact behavior depends upon whether the beam is modeled as extensional or inextensional, the type of intermediate support, and whether the natural frequencies are above or below the cut-off frequency.

2. Problem formulation

2.1. Harmonic wave solutions

Consider a thin curved beam, as shown in Fig. 1, where M is the bending moment, N the tensile force, and V the shear force. Neglecting the effects of rotary inertia, shear deformations, and damping, the coupled equations of motion governing the transverse (radial) displacement, W, and the tangential displacement, U, of the centroidal axis are

$$\frac{EI}{R^3}\frac{\partial^3}{\partial\theta^3}\left(U-\frac{\partial W}{\partial\theta}\right)-\frac{EA}{R}\left(W+\frac{\partial U}{\partial\theta}\right)=\rho AR\frac{\partial^2 W}{\partial T^2}, \tag{1a}$$

$$\frac{EI}{R^3}\frac{\partial^2}{\partial\theta^2}\left(U-\frac{\partial W}{\partial\theta}\right)+\frac{EA}{R}\frac{\partial}{\partial\theta}\left(W+\frac{\partial U}{\partial\theta}\right)=\rho AR\frac{\partial^2 U}{\partial T^2}, \tag{1b}$$

where E denotes the Young's modulus, I the second moment of inertia of the cross-section about the centroid, θ the angular coordinate, R the constant radius of curvature for the given range of angle θ, A the cross-sectional area, ρ the mass density, T the time variable. Details of deriving these equations of motion are found in Refs. [15,16].

Introduce the following non-dimensional variables and parameters:

$$u=\frac{U}{R},\quad w=\frac{W}{R}\quad t=\frac{T}{T_0},\quad T_0=R^2\sqrt{\frac{\rho A}{EI}}\quad k^2=\frac{I}{AR^2}, \tag{2}$$

where T_0 is a characteristic time constant and k is the curvature parameter [15]. Applying Eq. (2) to Eq. (1) yields the normalized equations of motion

$$k^2\frac{\partial^3}{\partial\theta^3}\left(u-\frac{\partial w}{\partial\theta}\right)-\left(w+\frac{\partial u}{\partial\theta}\right)=k^2\frac{\partial^2 w}{\partial t^2}, \tag{3a}$$

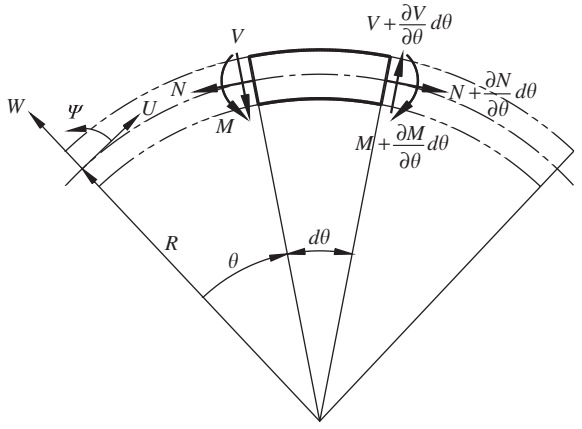

Fig. 1. Schematic of a curved beam and sign conventions.

$$k^2\frac{\partial^2}{\partial\theta^2}\left(u-\frac{\partial w}{\partial\theta}\right)+\frac{\partial}{\partial\theta}\left(w+\frac{\partial u}{\partial\theta}\right)=k^2\frac{\partial^2 u}{\partial t^2}. \tag{3b}$$

The equations for an inextensional curved beam are found by letting $w=-\mathrm{d}u/\mathrm{d}\theta$ [15]. In this case, Eq. (3) reduces to

$$\frac{\partial^3}{\partial\theta^3}\left(u-\frac{\partial w}{\partial\theta}\right)=\frac{\partial^2 w}{\partial t^2},\quad \frac{\partial^2}{\partial\theta^2}\left(u-\frac{\partial w}{\partial\theta}\right)=\frac{\partial^2 u}{\partial t^2}. \tag{4a, b}$$

In order to assess the wave propagation in the curved beam model, it is first necessary to determine the condition under which the following wave solutions

$$w(\theta,t)=C_w\mathrm{e}^{\mathrm{i}(\gamma\theta-\omega t)},\quad u(\theta,t)=C_u\mathrm{e}^{\mathrm{i}(\gamma\theta-\omega t)},\quad \mathrm{i}=\sqrt{-1},\quad 0\leqslant\theta\leqslant 2\pi \tag{5}$$

satisfy Eq. (3), where γ and ω are the non-dimensionalized wavenumber and frequency, respectively, and are defined as $\gamma=R\Gamma$ and $\omega=\Omega T_0$. Upon substituting the harmonic solutions in Eq. (5) into Eq. (3) and imposing the condition for non-trivial solutions, the dispersion equation for the extensional curved beam is found to be

$$\gamma^6-(2+k^2\omega^2)\gamma^4+\{1-(1+k^2)\omega^2\}\gamma^2+(k^2\omega^2-1)\omega^2=0. \tag{6}$$

Eq. (6) indicates that there are six wave components (three in each direction) exist governing the dynamics of the extensional curved beam in motion. Solving Eq. (6) for γ results in four different sets of roots, indicating that four distinct wave motions exist in an extensional curved beam depending on ω and k. These four harmonic wave motions are defined as [17]:

Case I (all six γ's are real): all wave components propagate.
Case II (two real γ's a and four complex γ's): two wave components propagate and four others are spatially varying.
Case III (two real γ's and four imaginary γ's): two wave components propagate and four others attenuate (near field components).
Case IV (four real γ'*s* and two imaginary γ's): four wave components propagate and two others attenuate.

The exact expressions of harmonic wave solution for these four cases can be found in Ref. [17]. It should be noted that there exists a non-zero *cut-off frequency*, ω_c, such that above this frequency the beam has coupled transverse (flexural) and tangential (extensional) modes, with the extensional mode dominating. This cut-off frequency is determined by taking the long-wavelength limit of Eq. (6), which gives $\omega_c=1/k$. This is the frequency when the wavelength of extensional waves in a straight rod is equal to $2\pi R$, and is known as the *ring frequency* in cylindrical shell dynamics [18].

2.2. Wave reflection and transmission

When a wave is incident upon a discontinuity such as an intermediate support, a different waveguide, or a boundary, it is reflected and/or transmitted at different rates depending on the properties of the discontinuity. A schematic of the system considered here is shown in Fig. 2.

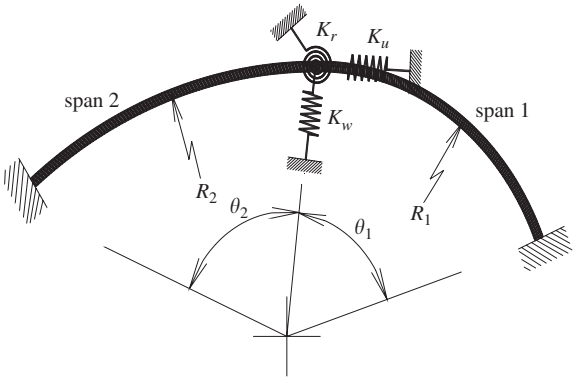

Fig. 2. Schematic of dual-span curved beam.

It consists of two sub-spans (spans 1 and 2) having a radius (R_1 and R_2) and span angle (θ_1 and θ_2). The sub-spans are attached by an intermediate support that consists of an elastic rotational constraint, K_r, an elastic transverse constraint, K_w, and an elastic tangential constraint, K_u. The tangential constraint is applicable since the curved beam is extensional. The non-dimensional elastic constrains are expressed as

$$k_u = \frac{K_u R_1^3}{EI}, \quad k_w = \frac{K_w R_1^3}{EI} \quad \text{and} \quad k_r = \frac{K_r R_1}{EI}. \tag{7}$$

The wave components are grouped into 3×1 vectors of positive-traveling waves $\mathbf{C}^+$ and negative-traveling waves $\mathbf{C}^-$; i.e.,

$$\mathbf{C}^+ = \{C_1^+ \;\; C_2^+ \;\; C_3^+\}^{\mathrm{T}}, \quad \mathbf{C}^- = \{C_1^- \;\; C_2^- \;\; C_3^-\}^{\mathrm{T}}. \tag{8a, b}$$

When a set of positive-traveling wave $\mathbf{C}^+$ is incident upon a discontinuity, it gives rise to a set of reflected waves $\mathbf{C}^-$ and transmitted waves $\mathbf{D}^+$. These waves are related by

$$\mathbf{C}^- = \mathbf{r}\mathbf{C}^+, \quad \mathbf{D}^+ = \{D_1^+ \;\; D_2^+ \;\; D_3^+\}^{\mathrm{T}} = \mathbf{t}\mathbf{C}^+, \tag{9a, b}$$

where $\mathbf{r}$ and $\mathbf{t}$ are the 3×3 reflection and transmission matrices, respectively. By imposing the geometric continuity and the force and moment balance conditions at the discontinuity, the wave reflection and transmission matrices, $\mathbf{r}$ and $\mathbf{t}$, can be obtained for each of the four *Cases* [17].

Now consider the curved beam elements to have different curvatures. Although the procedure described here remains the same, for simplicity, assume that the A, ρ, and E of the two beam elements are the same. Let the subscripts l and r denote the left and right sides, respectively, and $\sigma = R_r/R_l$ (curvature ratio). Then, the modified dispersion equation on the right side of the discontinuity is

$$\gamma_r^6 - (2 + \sigma^2 k^2 \omega^2)\gamma_r^4 + \{1 - (\sigma^2 + k^2)\sigma^2 \omega^2\}\gamma_r^2 + (\sigma^2 k^2 \omega^2 - 1)\sigma^4 \omega^2 = 0. \tag{10}$$

It is possible that a wave propagating on the left side becomes attenuating after crossing the discontinuity and vice versa. Hence, for an extensional curved beam, there are mathematically 16 (four in each span) possible combinations of wave motions to be considered. However, since Cases I and II have identical forms for their wave solutions, the actual number of combinations to

be considered is nine. The wave motion at boundaries can be determined in a similar manner as above [17].

2.3. Free vibration analysis

The wave reflection and transmission matrices are now combined with the transfer matrix method to analyze the free vibration of the curved beam with multiple discontinuities. The technique is known as the phase or wave-train closure principle, and it has been applied to straight beams [19–21]. Consider a curved beam with constant R with n discontinuities and arbitrary boundaries as shown in Fig. 3. Define $\mathbf{R}_i$ as a generalized reflection matrix which relates the amplitudes of negative and positive traveling waves at station (discontinuity) i and $\mathbf{T}_i$ as the field transfer matrix between station i and $i+1$ which relates the wave amplitudes by

$$\mathbf{w}^+(\theta_0+\theta)=\mathbf{T}\mathbf{w}^+(\theta_0) \text{ or } \mathbf{w}^-(\theta_0+\theta)=\mathbf{T}^{-1}\mathbf{w}^-(\theta_0). \tag{11}$$

Based on these definitions, the following relations can be found:

$$\mathbf{w}_n^- = \mathbf{R}_n\mathbf{w}_n^+ \quad (\mathbf{R}_n=\mathbf{r}_n), \tag{12}$$

$$\mathbf{w}_{ij}^- = \mathbf{R}_{ij}\mathbf{w}_{ij}^+ \quad \begin{cases} i=2,3,\ldots,n-1 \text{ (station \#)}, \\ j=l \text{ (left) or } r \text{ (right)}, \end{cases} \tag{13}$$

$$\mathbf{w}_1^- = \mathbf{T}_1\mathbf{w}_{2l}^-, \tag{14}$$

$$\mathbf{w}_1^+ = \mathbf{R}_1\mathbf{w}_1^- \quad (\mathbf{R}_1=\mathbf{r}_1), \tag{15}$$

$$\mathbf{w}_{2l}^+ = \mathbf{T}_1\mathbf{w}_1^+, \tag{16}$$

where in Eq. (13),

$$\mathbf{R}_{il}=\mathbf{r}_i+\mathbf{t}_i(\mathbf{R}_{ir}^{-1}-\mathbf{r}_i)^{-1}\mathbf{t}_i, \quad \mathbf{R}_{ir}=\mathbf{T}_i\mathbf{R}_{(i+1)l}\mathbf{T}_i. \tag{17a, b}$$

For waves traveling across a curvature change, the formulation of $\mathbf{R}_{il}$ requires particular attention. For example, if the wave motions in spans 1 and 2 are governed by

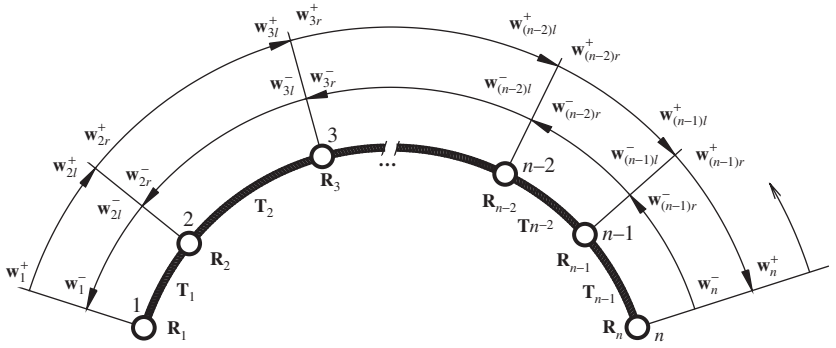

Fig. 3. Curved beam with multiple discontinuities and arbitrary boundary conditions.

Cases II and III, respectively,

$$\mathbf{R}_{2l} = \mathbf{r}_{\mathrm{II-III}} + \mathbf{t}_{\mathrm{III-II}}(\mathbf{R}_{2r}^{-1} - \mathbf{r}_{\mathrm{III-II}})^{-1}\mathbf{t}_{\mathrm{II-III}}. \tag{18}$$

Combining Eqs. (12)–(17),

$$(\mathbf{R}_1\mathbf{T}_1\mathbf{R}_{2l}\mathbf{T}_1 - \mathbf{I}_{3\times 3})\mathbf{w}_1^+ = 0. \tag{19}$$

Then, the frequency equation can be found from

$$C(\omega) = \mathrm{Det}[\mathbf{R}_1\mathbf{T}_1\mathbf{R}_{2l}\mathbf{T}_1 - \mathbf{I}_{3\times 3}] = 0. \tag{20}$$

The corresponding modeshapes can be also found in a similar manner by relating wave amplitudes between two adjacent sub-spans. The displacement at any point in the span i (or between station i and $i+1$) may have a form of

$$w_i(\xi) = \mathbf{T}_i(\xi)\mathbf{C}_i^+ + \mathbf{T}_i^{-1}(\xi)\mathbf{C}_i^-, \quad \theta_i \leqslant \xi \leqslant \theta_{i+1}, \tag{21}$$

where $\mathbf{C}_i^+$ and $\mathbf{C}_i^-$ denote the amplitudes of positive- and negative-traveling waves, respectively, in span i as in Eq. (8). Since

$$\mathbf{C}_i^- = \mathbf{R}_{ir}\mathbf{C}_i^+, \tag{22}$$

$$w_i(\xi) = (\mathbf{T}_i + \mathbf{T}_i^{-1}\mathbf{R}_{ir})\mathbf{C}_i^+. \tag{23}$$

Define $\mathbf{S}_i$ as a generalized transmission matrix which relates the amplitudes of incoming and outgoing waves at station i; i.e.,

$$\mathbf{C}_i^+ = \mathbf{S}_i\mathbf{C}_{i-1}^+, \tag{24a}$$

$$\mathbf{S}_i = (\mathbf{I}_{3\times 3} - \mathbf{r}_i\mathbf{R}_{ir})^{-1}\mathbf{t}_i\mathbf{T}_{i-1}. \tag{24b}$$

Combining Eqs. (23) and (24) gives the displacement of span i as a function of the wave amplitudes in span $i-1$:

$$w_i(\xi) = (\mathbf{T}_i + \mathbf{T}_i^{-1}\mathbf{R}_{ir})\mathbf{S}_i\mathbf{C}_{i-1}^+. \tag{25}$$

Assuming a disturbance arises in the first span, the modeshape of span i may then be generalized in terms of $\mathbf{C}_1^+$ as

$$w_i(\xi) = \{\mathbf{T}_i(\xi) + \mathbf{T}_i^{-1}(\xi)\mathbf{R}_{ir}\}\prod_{j=2}^{i}\mathbf{S}_j\mathbf{C}_1^+, \tag{26}$$

where the relationships among the three individual wave components C_k^+ ($k = 1, 2$, and 3) can be readily found in Eq. (19).

3. Results and discussion

The results for the first four modes are presented for various support conditions and curvatures. The transverse and tangential modes are determined for both the extensional and inextensional models. For each natural frequency, the corresponding modeshape and amplitude ratio for the

two sub-spans are determined. The amplitude ratio R_a is defined as

$$R_a = \begin{cases} \frac{|A_1|}{|A_2|}, & |A_1| < |A_2|, \\ \frac{|A_2|}{|A_1|}, & |A_2| \leqslant |A_1|, \end{cases} \tag{27}$$

where A_1 and A_2 are the maximum amplitude in each of the sub-spans. The amplitude ratio, which is determined for both the transverse and tangential modes, varies from 0 to 1. The smaller R_a is, the more localized the mode. In the context of mode localization, the modes will become highly localized if the sub-spans are weakly coupled and if there is a small disorder present in the system. For the curved beam model, a disorder can be introduced in two different ways. First, both sub-spans have the same radius ($R_1 = R_2$) but different span angles ($\theta_1 \neq \theta_2$). Second, both sub-spans can have different radii ($R_1 \neq R_2$) but the same span angle ($\theta_1 = \theta_2$). Both cases are considered here. In addition, the coupling between the spans will be mono-coupling (spans are coupled through only one of the elastic constraints). This will allow the effect of each type of elastic support to be studied individually.

For the extensional beam model, it is known that the behavior of the system above and below the cut-off frequency ω_c is physically different [17]. Because of this, the effect of the various elastic supports for an extensional beam system above and below ω_c will also be investigated. Upon choosing suitable parameters, it was found that for a total span angle ($\theta_t = \theta_1 + \theta_2$) of 80° and 170°, the first four natural frequencies for these two cases fall above and below ω_c, respectively. Unless otherwise specified, these angles and clamped boundary conditions are used in all subsequent calculations.

3.1. Effect of transverse support stiffness

In this section, the effects of k_w on the free response are studied. The parameters used in the following results are: curvature parameter $k = 0.1/\sqrt{12}$, and $R_1 = R_2$. To suppress direct extensional and rotational coupling (energy transfer) between the two sub-spans, let $k_u = k_r = \infty$. This will limit the coupling to the transverse motion of each span. Thus, the coupling effects due to the extensional mode are not directly present since $k_u = \infty$, however, the extensional effects do manifest themselves indirectly through the transverse motion due to the coupling between the transverse and tangential modes. The disorder here is introduced into the system through the sub-span angles. The disorder is chosen to be 0.5% of the total span angle θ_t. Therefore, for $\theta_t = 80°$, $\theta_1 = 40.4°$ and $\theta_2 = 39.6°$, and for $\theta_t = 170°$, $\theta_1 = 85.85°$ and $\theta_2 = 84.15°$. Figs. 4 and 5 show the amplitude ratio for the first four transverse and tangential modes of the extensional and inextensional curved beam models for varying k_w. The solid (filled) symbols are the extensional model. Fig. 6 shows some representative mode shapes along with the corresponding equilibrium configuration. It should be noted that these are the complete mode shapes; i.e., the sum of the tangential and transverse mode shapes.

In Fig. 4, the results for $\theta_t = 80°$ (all natural frequencies of the extensional model are above ω_c) are presented. The curves for the inextensional model are relatively flat and are clustered between 0.8 and 1.0, indicating that the transverse support stiffness appears to have a rather small effect on the modes. Fig. 4 also shows that modes 1 and 2 of the extensional model appear to be significantly more affected by the support stiffness than all of the other modes. The amplitude

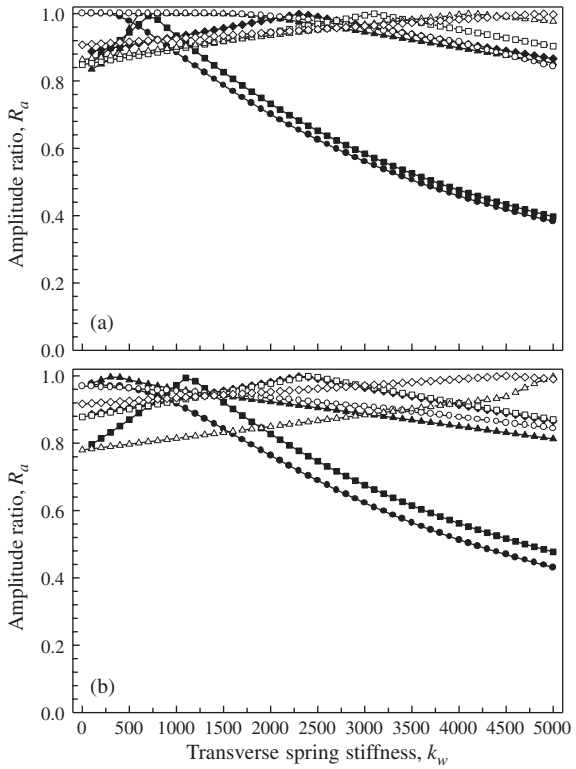

Fig. 4. Amplitude ratio versus k_w for $\theta_1 = 40.4^\circ$, $\theta_2 = 39.6^\circ$, $k_r = k_u = \infty$; inextensional (○, □, Δ, ◇), extensional (●, ■, ▲, ◆); mode 1 (●, ○), mode 2 (■, □), mode 3 (▲, Δ), mode 4 (◆, ◇); (a) transverse mode, (b) tangential mode.

ratio for these two modes decreases significantly as the support stiffness increases, resulting in the modes becoming more localized as the transverse support stiffness increases. This trend is observed for both the tangential and transverse modes.

In Fig. 5, the results for $\theta_t = 170^\circ$ (the first four natural frequencies of the extensional model are below ω_c) are shown. For $k_w > 1000$, the amplitude ratio of all of the modes decreases at the support stiffness increases. This suggests that both the extensional and inextensional models are significantly affected by the support stiffness, particularly as the support stiffness increases and becomes large. Fig. 5 also shows that certain modes have a similar qualitative and quantitative behavior. For example, both the transverse and tangential results show that the curves for modes 1 and 2 and modes 3 and 4 converge together as k_w becomes large. This is true for both the extensional and inextensional models. Thus, for large values of k_w, certain pairs of modes have almost identical amplitude ratios. The plots also indicate that the curves for modes 1 and 2 are nearly identical for both the inextensional and extensional models, which is true for both the transverse and tangential modes.

Also note that when comparing Figs. 4 and 5, it is seen that when the natural frequencies are below ω_c, both the extensional and inextensional models show the same qualitative trends with respect to the elastic support while when the natural frequencies are above ω_c they do not. It has

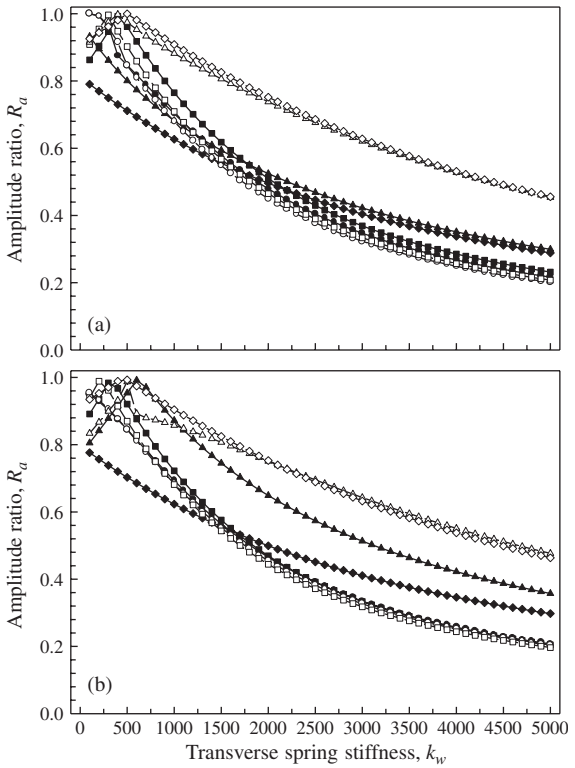

Fig. 5. Amplitude ratio versus k_w for $\theta_1 = 85.85^\circ$, $\theta_1 = 84.15^\circ$, $k_r = k_u = \infty$; inextensional (○, □, Δ, ◇), extensional (●, ■, ▲, ◆); mode 1 (●, ○), mode 2 (■, □), mode 3 (▲, Δ), mode 4 (◆, ◇); (a) transverse mode, (b) tangential mode.

been shown that, in general, the behavior of single-span inextensional and extensional curved beam models below ω_c are very similar, with each model exhibiting modes which are primarily flexural [17]. Thus, with respect to the behavior of curved beams above and below the cut-off frequency, both the single-span curved beam and the dual-span curved beam exhibit similar characteristics.

3.2. *Effect of tangential support stiffness*

The effects of k_u on the amplitude ratio are presented using the same parameters as those in the previous section with $k_w = k_r = \infty$. In this case, the energy transfer between the sub-spans is directly through the extensional mode only. Figs. 7 and 8 show the amplitude ratio for a total span angle of 80° and 170°, respectively, with varying k_u. Fig. 9 shows some representative modeshapes for a total span angle of 170°.

In Fig. 7, the amplitude ratio for the inextensional model, in general, varies between 0.1 and 1 for all four modes, with the amplitude ratio decreasing as k_u increases. The extensional results show a much different trend than those of the inextensional model. First, it is noticed that the amplitude ratio curves for modes 1 and 4 and modes 2 and 3 are paired together and

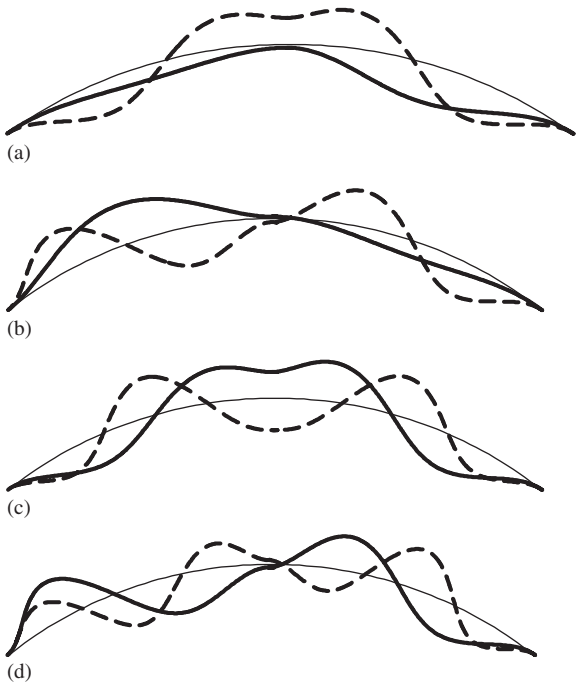

Fig. 6. First four mode shapes for $\theta_1 = 40.4^\circ$, $\theta_2 = 39.6^\circ$, $k_r = k_u = \infty$, $k_w = 5000$; extensional (——), inextensional (------); (a) mode 1, (b) mode 2, (c) mode 3, (d) mode 4. The thin solid line denotes the equilibrium configuration.

follow the same trend as k_u increases. While modes 1 and 4 experience little or no localization, modes 2 and 3 are highly localized. Moreover, the amplitude ratio for modes 2 and 3 are nearly identical.

In Fig. 8, it is again seen that the modes tend to be paired together and have similar behavior. For the extensional model, the pairing of modes depends whether k_u is above or below some critical value. For example, it is seen that for $k_u \leqslant 2500$, modes 2 and 3 and modes 1 and 4 are paired together. However, for $k_u > 2500$, modes 1 and 2 and modes 3 and 4 are paired together. This same behavior is also observed for the inextensional model. This complex behavior is believed to be attributed in part to the fact that below ω_c (Fig. 8) there exits the possibility of three different types of wave motions (Cases I, II or III) for the extensional model. However, above ω_c (Fig. 7), the extensional model is governed by only one wave motion (Case IV). It should also be noted that both the extensional and inextensional models are governed by the same three wave motions (Cases I, II or III) below the cut-off frequency. Thus, the qualitative behavior of the extensional and inextensional models below the cut-off frequency is expected to be similar, as seen in Figs. 8 and 9.

Comparing Figs. 7 and 8, it is observed that the general trends for the curves in each plot are quite different, indicating that the effect of the tangential constraint on each system is different. In Fig. 7, modes 1 and 4 and modes 2 and 3 of the extensional model have very similar behavior. However, in Fig. 8, modes 1 and 2 and modes 3 and 4 have similar behavior. This observed behavior is seen to occur for both the transverse and tangential modes. The results seen here

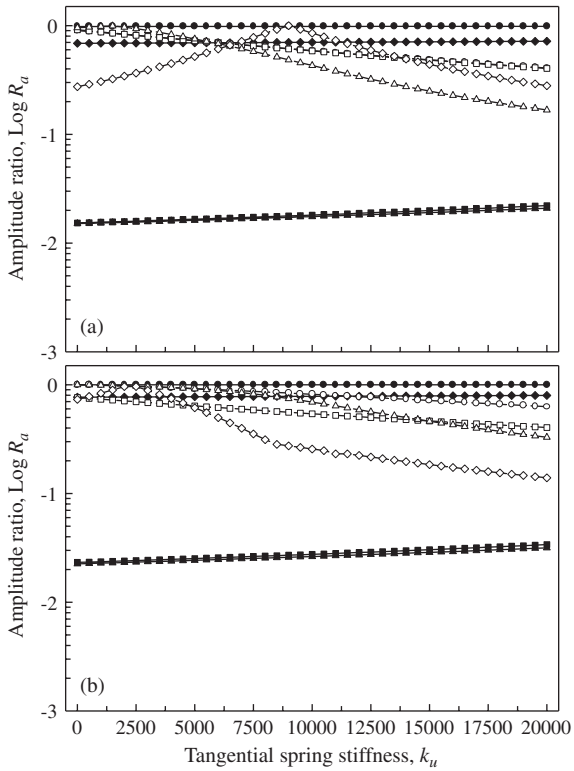

Fig. 7. Amplitude ratio versus k_u for $\theta_1 = 40.4^\circ$, $\theta_2 = 39.6^\circ$, $k_r = k_w = \infty$; inextensional (○, □, Δ, ◇), extensional (●, ■, ▲, ◆); mode 1 (●, ○), mode 2 (■, □), mode 3 (▲, Δ), mode 4 (◆, ◇); (a) transverse mode, (b) tangential mode.

suggest that for the tangential constraint, the behavior of a particular mode or pair of modes depends upon whether the natural frequencies are above or below the cut-off frequency.

In comparing all of the above figures, several things are observed regarding the effect of the support stiffness on the amplitude ratio. First, the general behavior of the curves for each type of elastic support is different, indicating that each elastic support affects the curved beam models differently. Second, the general trends for the beam system above and below the cut-off frequency are noticeably different. This suggests that the affect of the support depends strongly upon whether the natural frequency of the system is above or below the cut-off frequency. Third, the trends observed for the transverse and tangential modes are very similar. Thus, practically speaking, for both the extensional and inextensional models, it is only necessary to study either the tangential or transverse modes to assess the qualitative affects of the support stiffness.

3.3. Frequency loci

Another way to assess the coupling between the two sub-spans is to plot the natural frequencies versus the disorder. The disorder here is introduced through the sub-span angles ($R_1 = R_2, \theta_1 \neq \theta_2$). Figs. 10 and 11 show the frequency loci curves for the first four modes with $k_r = 500$, $k_u = k_w = \infty$

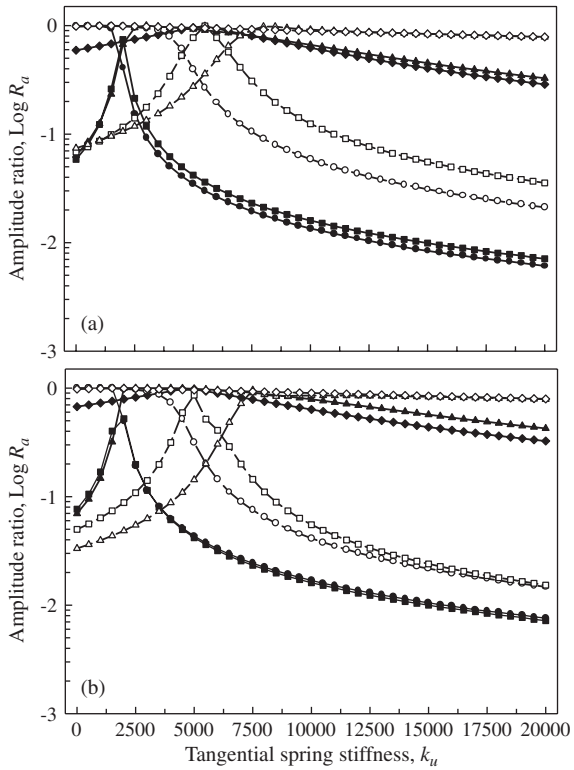

Fig. 8. Amplitude ratio versus $\theta_1 = 85.85^\circ$, $\theta_1 = 84.15^\circ$, $k_r = k_w = \infty$; inextensional (○, □, Δ, ◇), extensional (●, ■, ▲, ◆); mode 1 (●, ○), mode 2 (■, □), mode 3 (▲, Δ), mode 4 (◆, ◇); (a) transverse mode, (b) tangential mode.

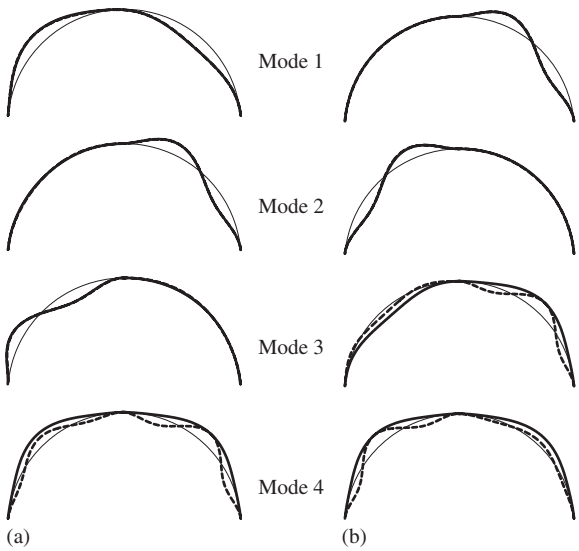

Fig. 9. First four modeshapes for $\theta_1 = 85.85^\circ$, $\theta_1 = 84.15^\circ$,and $k_r = k_w = \infty$; extensional (——), inextensional (- - - -); (a) $k_u = 1000$, (b) $k_u = 19\,500$. The thin solid line denotes the equilibrium configuration.

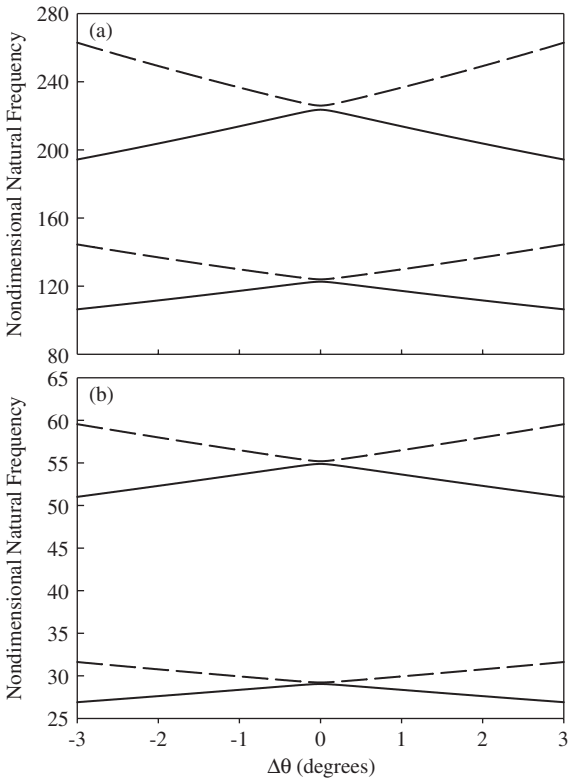

Fig. 10. Frequency loci curves for the inextensional model with $k_u = k_w = \infty$, $k_r = 500$; modes 1 and 3 (——), modes 2 and 4 (– – –); (a) $\theta_t = 80^\circ$, (b) $\theta_t = 160^\circ$.

for the inextensional and extensional models, respectively. The horizontal axis represents the amount of angular disorder ($\Delta\theta$) present in the system, i.e., when $\theta_1 = \theta_2$, $\Delta\theta = 0$.

For the inextensional model, Fig. 10 shows the frequency loci curves for total span angles of 80° and 160°. Both plots exhibit curve veering and have similar behavior. In particular, the veering occurs in pairs, namely, modes 1 and 2 and modes 3 and 4. In the regions where this curve veering occurs, the modes are highly localized. It is well known that eigenvalue curve veering occurs for weakly coupled, nearly periodic systems, and associated with this curve veering is a strong localization of the modes known as mode localization [10]. In fact, the behavior exhibited in Fig. 10 is typical of many weakly coupled, nearly periodic systems [10,14]. In Fig. 11, the frequency loci curves for total span angles of 80° and 160° for the extensional model are shown. It should be noted that the cut-off frequency is $\omega_c = 34.64$. Thus, the first four natural frequencies for the 80° total span angle are above ω_c and the first four natural frequencies for the 160° total span angle are below ω_c for the given range of $\Delta\theta$. Again, in the regions of curve veering, the modes are highly localized. It is clear from the figures that the behavior of the system above and below ω_c is quite different.

The complex frequency veering exhibited by the extensional model below the cut-off frequency in Fig. 11(b) is due to the fact that the extensional curved beam system has two coupling mechanisms. The first mechanism is the inter-span coupling between adjacent spans which is due to the rotational spring k_r. The second mechanism is the inherent intra-span coupling between the

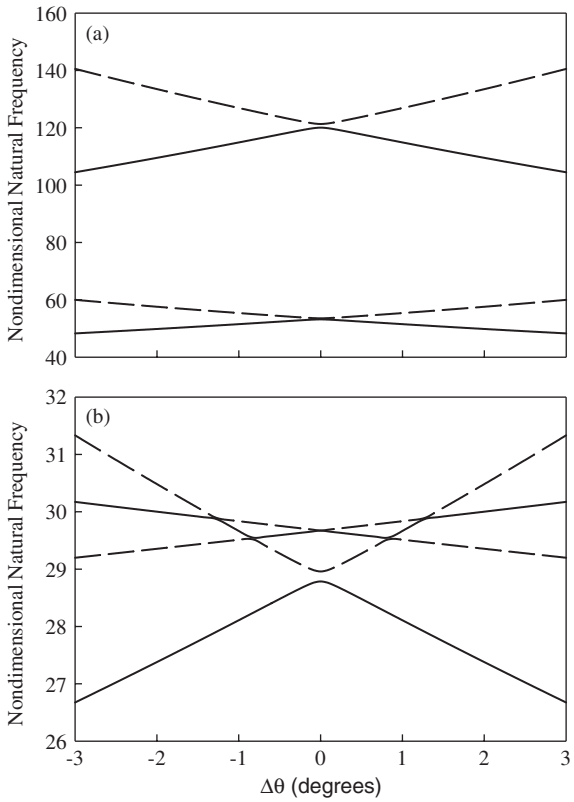

Fig. 11. Frequency loci curves for the extensional model with $k_u = k_w = \infty$, $k_r = 500$; modes 1 and 3 (——), modes 2 and 4 (– – –); (a) $\theta_t = 80^\circ$, (b) $\theta_t = 160^\circ$.

flexural (transverse) and extensional (tangential) modes due to the extensibility of the neutral axis. Based on the definition of mode localization, a periodic or nearly periodic system exhibits strongly localized modes if the system is weakly coupled and contains a small disorder. While the first coupling mechanism provides the necessary condition for mode localization, the second coupling mechanism acts to augment the coupled behavior produced by the first mechanism.

The effect of the second coupling mechanism can be seen in Fig. 12, which shows the transverse amplitude ratio for the extensional and inextensional models for varying k_r. Note that Figs. 11(a) and 12(a) present results above the cut-off frequency and Figs. 11(b) and 12(b) present results below the cut-off frequency. From Fig. 12(a), it can be seen that the amplitude ratio of the first four modes of the extensional and inextensional models above the cut-off frequency are all nearly identical (all curves overlap). However, below the cut-off frequency (Fig. 12(b)), the amplitude ratio of the four inextensional modes and the first and second extensional modes are nearly identical, while the amplitude ratio of the third and fourth modes of the extensional are significantly lower (more strongly localized). This decrease or shift in amplitude ratio of the third and fourth extensional modes in Fig. 12(b) is due to second coupling mechanism shown in Fig. 11(b). Thus, based on the results here, the second mechanism appears to amplify the mode localization.

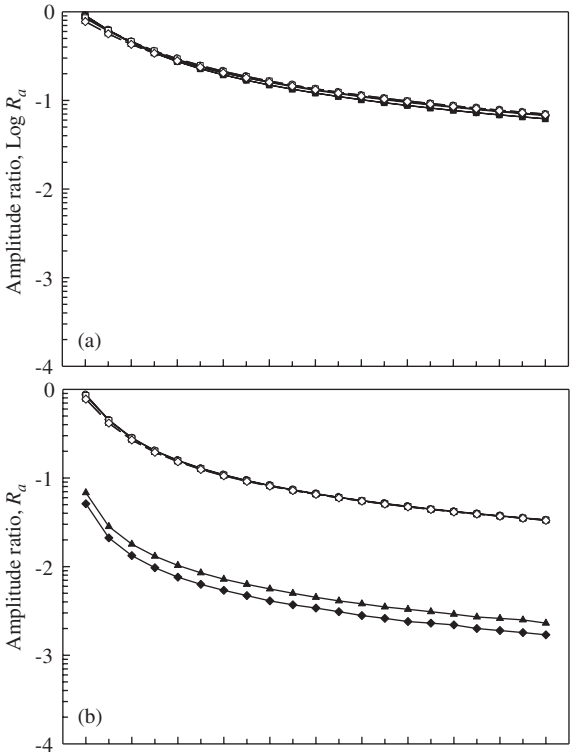

Fig. 12. Transverse amplitude ratio versus k_r for $k_u = k_w = \infty$; inextensional (○, □, Δ, ◇), extensional (●, ■, ▲, ◆); mode 1 (●, ○), mode 2 (■, □), mode 3 (▲, Δ), mode 4 (◆, ◇); (a) $\theta_1 = 40.4^\circ$, $\theta_2 = 39.6^\circ$, (b) $\theta_1 = 85.85^\circ$, $\theta_1 = 84.15^\circ$.

It should be noted that this second coupling mechanism is only present in the extensional model and not the inextensional model since it is the extensibility of the neutral axis which couples the transverse and tangential modes. Also, while the second coupling mechanism is always present in the extensional model, the extent to which it will influence the first coupling mechanism appears to depend upon whether the natural frequencies are above or below the cut-off frequency. For all of the various cases considered in this study, the second coupling mechanism affected only those natural frequencies that were below the cut-off frequency. It is therefore believed that the effect of the second coupling mechanism on the mode localization of natural frequencies above the cut-off frequency is negligible. While other factors such as curvature and boundary conditions may alter the characteristics of the second coupling mechanism, the effects of these factors are not addressed here. Thus, the results here confirm that there can be a significant difference in the coupled behavior of the extensional and inextensional models.

3.4. Effect of curvature

The results in this section focus on how the curvature affects the response of the curved beam model. First, a disorder is introduced into the system through the sub-span radii. That is, $\theta_1 = \theta_2$ but $R_1 \neq R_2$. As seen from Eqs. (3) and (4), while the equations for the extensional curved beam

model contain the curvature parameter k, the equations for the inextensional curved beam model do not. Thus, the inextensional curved beam model is independent of k (and hence R). As a result, the radii imperfection $R_1 \neq R_2$, while affecting only the inter-span coupling for the inextensional curved beam model, will affect both the inter- and intra-span coupling of the extensional curved beam model. Therefore, for the inextensional curved beam model, the radii disorder will have a qualitatively similar behavior as the angular disorder presented in the previous sections. For this reason, the behavior of extensional curved beam model is the focus of this section and only results pertaining to it are presented here.

The case of $k_r = 1000$, $k_u = k_w = \infty$ is presented in Fig. 13 which shows the amplitude ratio versus the ratio of the radii as well as the natural frequencies of the system. Representative

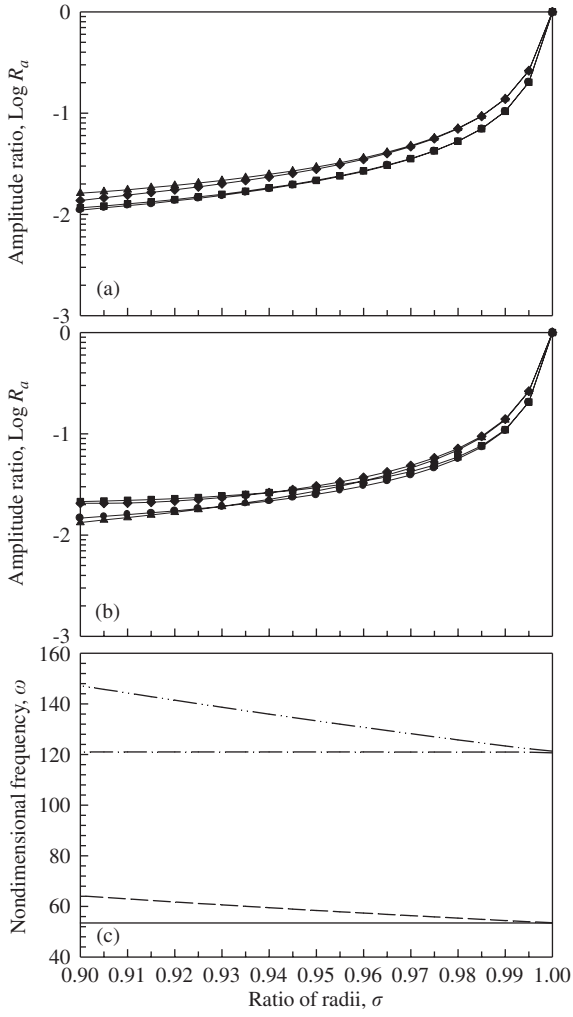

Fig. 13. Amplitude ratio versus radii ratio for $\theta_1 = \theta_2 = 40^\circ$, $k_u = k_w = \infty$, $k_r = 1000$; mode 1 (—), mode 2 (– – –), mode 3 (– · – · –), mode 4 (– · · – · · –); (a) transverse mode, (b) tangential mode, (c) nondimensional natural frequency.

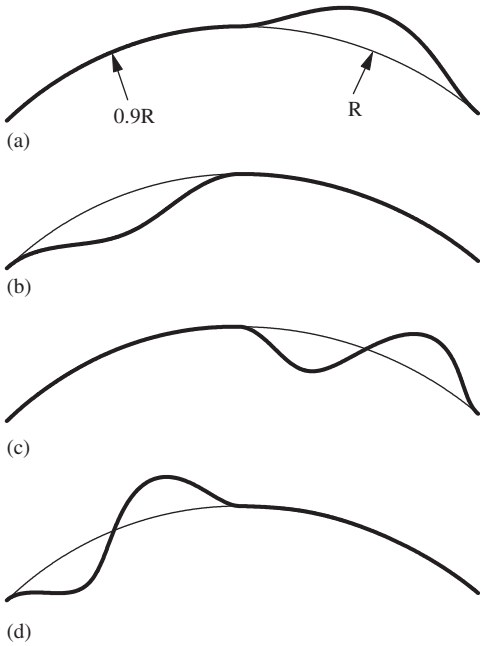

Fig. 14. First four modeshapes for $\theta_1 = \theta_2$, $\sigma = 0.9$, $k_u = k_w = \infty$, $k_r = 1000$; (a) mode 1, (b) mode 2, (c) mode 3, (d) mode 4. The thin solid line denotes the equilibrium configuration.

modeshapes are shown in Fig. 14. It is observed that as the radii of each span become slightly different, the amplitude ratio becomes quite small, indicating that the modes are highly localized. Fig. 13 also shows that over the range of σ considered, the natural frequencies of modes 1 and 3 are nearly constant while modes 2 and 4 are substantially changed by the disorder. Although the frequencies of modes 1 and 2 remain nearly constant, it is interesting to note that the amplitude ratio of modes 1 and 2 decrease significantly. Thus, it appears that the radii disorder can affect the natural frequency of each mode differently.

4. Conclusion

The free vibration response of dual-span circular curved beams constrained by an intermediate elastic support is studied. The curved beams are modeled as either extensional or inextensional with the intermediate elastic constraint consisting of a transverse, tangential and rotational spring. The eigenvalue problem is formulated using wave propagation techniques in conjunction with the wave-train closure principle. Because both propagating and attenuating wave are included in the analysis, the results are exact. The effects of the support type and stiffness on the transverse and tangential modes are examined. It is found that each type of elastic support affects the response of the coupled system differently. This is true for both the extensional and inextensional curved beam models. In addition, for the extensional model, the behavior also depends upon whether the natural frequencies of the system are above or below the cut-off frequency. This is due in part to

the inherent coupling that exists between the transverse and tangential modes, which exists only in the extensional curved beam model. Both the span angle disorder and the radii disorder produce highly localized modes, and in general, each mode is affected differently. Under certain conditions, however, particular pairs of modes of the extensional and inextensional models have very similar behavior. For both extensional and inextensional models, trends observed for the transverse and tangential modes are nearly identical.

References

[1] P. Chidamparam, A.W. Leissa, Vibration of planar curved beams, rings, and arches, *Applied Mechanics Review* 46 (1993) 467–483.
[2] P.A.A. Laura, M.J. Maurizi, Recent research on vibrations of arch-type structures, *Shock and Vibration Digest* 19 (1987) 6–9.
[3] S. Markus, T. Nanasi, Vibration of curved beams, *Shock and Vibration Digest* 13 (1981) 3–14.
[4] Y. Wasserman, Spatial symmetrical vibrations and stability of circular arches with flexibly supported ends, *Journal of Sound and Vibration* 59 (1978) 181–194.
[5] T.M. Wang, J.M. Lee, Natural frequencies of multi-span circular curved frames, *International Journal of Solids and Structures* 8 (1972) 791–805.
[6] C.P. Filipich, R. Carnicer, V.H. Cortinez, P.A.A. Laura, In-plane vibrations of a circumferential arch elastically restrained against rotation at one end and with an intermediate support, *Applied Acoustics* 22 (1987) 261–270.
[7] M. Petyt, C.C. Fleischer, Vibration of multi-supported curved beams, *Journal of Sound and Vibration* 32 (1974) 359–365.
[8] C.G. Culver, D.J. Oestel, Natural frequencies of multispan curved beams, *Journal of Sound and Vibration* 10 (1969) 380–389.
[9] O.O. Bendiksen, Mode localization phenomena in large space structures, *AIAA Journal* 25 (1987) 1241–1248.
[10] C. Pierre, D.M. Tang, E.H. Dowell, Localized vibrations of disorderd multispan beams: theory and experiment, *AIAA Journal* 25 (1987) 1249–1257.
[11] N. Al-Jawi, A.G. Ulsoy, C. Pierre, Vibration localization in band-wheel systems: theory and experiment, *Journal of Sound and Vibration* 179 (1995) 289–312.
[12] S.D. Lust, P.P. Friedmann, O.O. Bendiksen, Mode localization in multispan beams, *AIAA Journal* 31 (1993) 348–355.
[13] B. Kang, C.A. Tan, Transverse mode localization in a dual-span rotating shaft, *Journal of Sound and Vibration* 219 (1999) 133–155.
[14] C.H. Riedel, C.A. Tan, Dynamic characteristics and mode localization of elastically constrained axially moving strings and beams, *Journal of Sound and Vibration* 215 (1998) 455–473.
[15] P. Chidamparam, A.W. Leissa, Influence of centerline extensibility on the in-plane free vibrations of loaded arches, *Journal of Sound and Vibration* 183 (1995) 779–795.
[16] K.F. Graff, *Wave Motion in Elastic Solids*, Ohio State University Press, 1975.
[17] B. Kang, C.H. Riedel, C.A. Tan, Free vibration of planar curved beams by wave propagation, *Journal of Sound and Vibration* 260 (2003) 19–44.
[18] S.J. Walsh, R.G. White, Vibrational power transmission in curved beams, *Journal of Sound and Vibration* 233 (2000) 455–488.
[19] C.A. Tan, B. Kang, Free vibration of axially loaded, rotating Timoshenko shaft systems by the wave-train closure principle, *International Journal of Solids and Structures* 36 (1999) 4031–4049.
[20] D.J. Mead, Waves and modes in finite beams: application of the phase-closure principle, *Journal of Sound and Vibration* 171 (1994) 695–702.
[21] B.R. Mace, Wave reflection and transmission in beams, *Journal of Sound and Vibration* 97 (1984) 237–246.